Dynamics of Continuous, Discrete and Impulsive Systems
Series **B:** *Applications & Algorithms* **26 (2019)** 153-170

INTEGRATING HAWKES PROCESS- AND BIOMASS MODELS TO CAPTURE IMPULSIVE POPULATION DYNAMICS

Tomoyuki Nakagawa[1], Sam Subbey[2,3], and Hiroko K. Solvang[2]

[1]Department of Mathematics, Graduate School of Science, Hiroshima University,
1-3-1 Kagamiyama Higashi-Hiroshima Hiroshima, 739-8526, Japan

[2]Institute of Marine Research,
PB-1870, N-5817 Bergen, Norway (samuels@imr.no)

[3]Cornell University, Department of Natural Resources, Room 120 Fernow Hall,
Ithaca, NY 14853, USA (ss2223@cornell.edu)

Abstract. This paper presents a modeling framework that captures the impulsive biomass dynamics (bust-boom) of a fish stock. The framework is based on coupling a Hawkes-process model to a discrete-time, ages-structured population dynamics model. Simulation results are presented to demonstrate the efficacy of the framework in capturing impulsive events in the population trajectory.
The results presented in this paper are significant in three ways:

- A framework has been presented that demonstrates how premonitory information may be extracted from exogenous observations from complex environmental systems
- We have demonstrated how exogenous information may be parameterized and incorporated into the modeling process for better understanding of the link between environmental drivers and the population dynamical system
- The framework has been successfully applied in modeling and short-term prediction of the population dynamics of an empirical fish stock.

Keywords. Hawkes process, Discrete time, Delay-time model, Auto-regressive, Impulsive population dynamics, Marine population, Parameter estimation.

AMS (MOS) subject classification: 93A30, 92-08, 90C31

1 Introduction

This paper deals with a system consisting of a single prey (the Barents Sea capelin) and multiple predators in a real ecosystem, where the prey biomass is impulsive, and a period of boom is followed by a protracted period of bust. No unique theory (based on predator-prey considerations) exists currently, to explain the multiple bouts of population bust and boom that has been observed in the past three decades, see e.g., [5, 15]. The goal of this paper is to investigate a hypothesis that considers an environmental point process as an external forcing of the population biomass dynamics. The approach involves

using extracted information from environmental observations to inform when future population levels will either be stationary (connected to non-volatile state of the environmental driver), or nonstationary (linked to an unbounded number of environmental process events) [2, 12]. In the simplest case, we consider the point process to be self-exciting (the probability of a future event increases with the occurrence of past events), and that the conditional expectation for occurrence of an event at each time is linear. Such a system can be viewed as a Poisson cluster process, or more specifically, as a linear Hawkes process [13]. We present a framework that couples the environment (through a parameterized point process (Hawkes) model) to a population dynamics model, to provide short-term predictions of the population trajectory.

In the Barents Sea (BS), capelin is a short-lived (1–4 years) fish species, that is considered to be the most important fish stock [6]. It is the main prey for Northeast Arctic cod [1, 8] and juvenile herring [11]. Several marine mammals (e.g. harp seals, humpback whales, minke whales), seabirds, kittiwakes and guillemots are also known to prey on capelin. The capelin stock has undergone three population collapses during the periods 1985–1989, 1993–1997, 2003–2006 [8], and it is currently in a fourth collapse period, which started in 2015 [8].

Several hypotheses have been proposed to explain the underlying mechanisms for the stock collapse [5, 15]. What has become accepted, is the inability of the stock to replenish itself (referred to as recruitment failure) due mainly to high levels of predation from other species during crucial capelin life stages [10]. The dynamics of the capelin stock has therefore be described as being dominated by a top-down control because the stock dynamics is regulated by predation pressure from species higher up in the foodchain. This explanation for stock decline and collapse is consistent with classical ecological theory, and appears to hold true for most observation years. The literature also shows a divergence from the accepted theory about top-down regulation of the capelin population dynamics. During some observation years, large (key) predator and prey populations have been noted to have coexisted, with insignificant effects on the prey population biomass [9]. The divergence from theory implies the existence of other plausible hypotheses for the dynamics of the capelin biomass. According to an alternative hypothesis [33], the fluctuation of the capelin fish stock (rather than being a top-down regulatory system) is a natural adaptation to the environment and a strategy for optimal growth and survival in the long run. In [33] the fluctuations of the capelin stock was referred to as *stochastic resonance*. This resonance was characterized by a periodicity of 6.2 years, and linked to the *lunar nodal tide*, which in turn, is supposed to affect the variability of sea level, temperature, and salinity in the BS [34]. A more recent paper by [31] analyzed the capelin biomass data and those of its key predators. This paper showed that the dynamics of the capelin biomass appears to be predominantly periodic (with a periodicity $\tau \geq 5$ years) and autonomous. The findings in [31] appear to be partially consistent with those in [33]. Both papers allude to regulation

of the capelin biomass by exogenous system drivers, rather than the classical predator-prey system dynamics.

Motivated by [31] and [33], this paper investigates the alternative hypothesis that the dynamics of capelin biomass is characterized by a bottom-up regulatory process, where food is considered as the main driver explaining population fluctuations. In contrast to [33], we do not consider exogenous factors (e.g. lunar nodal tide and temperature) as direct drivers, but as proxies for food. The hypothesis investigated in this paper does not discount that the populations dynamics may be regulated by both top-down, and bottom-up processes. This may occur for instance, through a seasonal shift from one process to the other, or through both processes acting in concert in space and time.

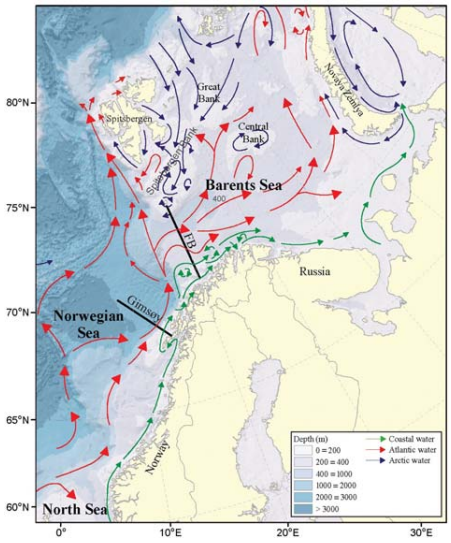

Figure 1: Schema of main currents in the BS, and location of the FB section.

In the approach developed in this paper, we use different formulations of autoregressive models to represent the autonomous dynamical system of the capelin biomass. We use a proxy for food to identify event times associated with elevated growth in the stock biomass. Zooplankton (copepods, euphausiids, amphipods) are the major prey item for BS capelin [3]. Major zooplankton communities are associated with influx of different water masses of Atlantic, and Arctic origins. The volume flux of Atlantic water into the BS is measured along a standard section namely, the Fugløya-Bear Island (FB) transect, located at the western entrance to of the BS (see Figure 1). According to [3], over 50% of the FB zooplankton density in late summer can be explained by a regression model that uses only volume flux of Atlantic water (AW) across the FB transect. Since it is this biomass that is advected into

the BS to serve as food for capelin (among others), we consider the volume flux of AW as proxy for food level. By considering the flow of AW into the BS as generated by a self-regulating process, we describe the volume flux (proxy for food) by a self-exciting model, with distinct excitation times. By linking a Hawkes process to the AR biomass model, we develop a framework for modeling the observed bust-boom dynamics of the capelin stock, where boom periods are defined by the self-excitation model.

The rest of the manuscript is organized in the following way. Section 2 gives a brief background to the modeling framework. This section presents the self-exciting (Hawkes) model that uses exogenous volume flux observations to provide premonitory information about the population trajectory, and the system of autoregressive models that describe the population dynamics. Section 3 summarizes the computational and parameter estimation procedures, while Section 4 describes how the modeling framework is applied to an empirical ecological problem. We present final discussion of our results in Section 5, including their significance in an ecological perspective.

2 Point Process and Population Dynamics Models

2.1 The Hawkes Process Model

A Hawkes Process (HP) model [12] is a mathematical description for stochastic point process, self-exciting phenomena. The HP is a non-Markovian extension of the Poisson process [22].Mathematically, a point (counting) process function $N(t)$ is a Hawkes process satisfying (1) and (2), where Pr stands for probability and t represents time.

$$\begin{aligned} \Pr\{N(t+\delta) - N(t) = 1 | N(s)(s \leq t)\} &= \Lambda(t)\delta + o(\delta), \quad (1) \\ \Pr\{N(t+\delta) - N(t) > 1 | N(s)(s \leq t)\} &= o(\delta), \quad (2) \end{aligned}$$

where $\Lambda(t)$ is referred to as the intensity function, which satisfies (3).

$$\begin{aligned} \Lambda(t|\boldsymbol{\theta}) &= \lambda + \int_{-\infty}^{t} g(t-u|\boldsymbol{\theta}_p) dN(u), \quad (3) \\ \boldsymbol{\theta} &\equiv (\lambda, \boldsymbol{\theta}_p). \end{aligned}$$

We define for some $d \in \mathbb{N}_{>0}$, $\boldsymbol{\theta} \in \mathbb{R}^d$, $\lambda > 0$, and the response function $g(t) \geq 0$. The function g is left continuous for $t \geq 0$ and $\int_0^\infty g(t)dt < 1$.

Given a sequence of event times $t_1, \ldots, t_n$ in the interval $[0, T \geq t_n]$, the log-likelihood ℓ_H of a point process with an intensity function $\Lambda(t)$ is given by (see [25]) (4).

$$\ell_H(t_1, \ldots, t_n|\boldsymbol{\theta}) = -\int_0^T \Lambda(t|\boldsymbol{\theta})dt + \int_0^T \log \Lambda(t|\boldsymbol{\theta}) dN(t). \quad (4)$$

Equation (5) defines the response function $g(t)$ adopted in this paper, which is an instance of exponentially decaying response.

$$\begin{aligned} g(t|\boldsymbol{\theta}_p) &= \alpha e^{-\beta t}, \\ \boldsymbol{\theta}_p &\equiv (\alpha, \beta),\ \alpha > 0,\ \beta > 0\ \alpha < \beta. \end{aligned} \tag{5}$$

For this particular choice of $g(t)$, an exact form of the log-likelihood function (see [25, 28] for derivation details) is given by (6).

$$\begin{aligned} \ell_H(t_1, \ldots, t_n|\boldsymbol{\theta}) &= -\lambda T + \sum_{i=1}^{n} \left[\frac{\alpha}{\beta} \left(e^{\beta(t_i - T)} - 1 \right) + \log\left(\lambda + \alpha A(i)\right) \right], \\ A(i) &= \sum_{t<t_i} e^{-\beta(t_i - t)},\ \text{for } i \geq 2, \end{aligned} \tag{6}$$

where $T = t_n$, $A(1) = 0$, and t_i denotes the occurrence time for the ith event.

In this paper, we use the volume flux of AW into the BS to determine the event times for the Hawkes process, and an optimization algorithm to determine the maximum likelihood estimates (MLE) $\hat{\boldsymbol{\theta}}$, of $\boldsymbol{\theta}$ in (6).

2.2 Defining a Population Dynamics Model

This paper considers the three classes of models (AR, ARX, and mmAR) in linking the environment (through the intensity function) to the biomass dynamics.

Autoregressive (AR) models are useful tools for dynamical system modeling when observations are recorded at discrete times (time series) [26, 29]. Autoregressive models with exogenous terms (ARX), and Multiplicatively modulated AR (mmAR) models are extensions of AR models to allow for inclusion of exogenous variables. An ARX model incorporates exogenous variables by additive terms to an AR model [29]. In the case of an mmAR model, the influence of the exogenous variables are expressed through the coefficients of the AR model [21].

Suppose in general, that $\boldsymbol{B} \equiv \{B_1, \ldots, B_N\}$ is a random variable (e.g., representing the time series of population size) whose dynamics we intend to model. Define $\{e,\ f\} \subset \mathbb{N}_{>0} : e \leq f$, and let $\boldsymbol{X} \in \mathbb{R}^e$ be a vector of random variables derived from exogenous or environmental observations, $\tilde{\boldsymbol{x}} \in \mathbb{R}^f$. The exact form for $\boldsymbol{X}$ will be defined later. For $j = 1, 2, \ldots$ and $n = 1, 2, \ldots, N$, where $M \leq N \leq M+e$, we define the following three models,

$$B_n = \begin{cases} \sum_{m=1}^{M} a_m B_{n-m} + \epsilon_n, & \text{AR}, \\ \sum_{m=1}^{M} a_m B_{n-m} + b_j X_{n-j} + \epsilon_n, & \text{ARX}, \\ \sum_{m=1}^{M} (a_m + b_{m,j} X_{n-j}) B_{n-m} + \epsilon_n & \text{mmAR}, \end{cases} \tag{7}$$

where M is the AR order, a_m, b_j and $b_{m,j}$ are AR coefficients and the coefficient of exogenous variables, and ϵ_n is normally distribution with zero mean and variance σ^2.

2.3 Event Time Detection

Assume that we are given the environmental observations $\boldsymbol{x}(t) \equiv \{x_1, \ldots, x_f\}$, with corresponding time series of observation times $\boldsymbol{T} = \{t_1, t_2, \ldots, t_f\}$, where $x_j = \boldsymbol{x}(t_j)$, $j = 1, \ldots, f$. The goal is to use a sliding time-window on $\boldsymbol{x}(t)$, to define event times associated with significant deviations in the value of $\boldsymbol{x}(t)$. We define a time window length, ψ, for t, and threshold bounds, $[\omega_1\ \omega_2]$, for $\boldsymbol{x}(t)$. By sliding the window along the time axis, we define (for $j = 1, \ldots, n \leq f$) any $\tau_j \in \boldsymbol{T}$ as an event time if $\boldsymbol{x}(\tau_j) \geq \omega_2$ or $\boldsymbol{x}(\tau_j) \leq \omega_1$.

For $\tau_1 < \tau_2 <, \ldots, < \tau_n$, the n-ordered set $\boldsymbol{T}_e \subseteq \boldsymbol{T} : \boldsymbol{T}_e = \{\tau_1\ \tau_2\ \ldots\ \tau_n\}$, defines the event times for the Hawkes process. This paper uses the Peakfinder algorithm (see example usage in [23]) in identifying event times.

2.4 Definition of X_n

The influence of the exogenous variable (parameterized by $g(t)$) has been assumed to exponentially decay with time. However, the intensity level and duration of the influence, is determined by the functional parameter set $\boldsymbol{\theta} \equiv \{\alpha\ \beta\}$, in (5). The optimal parameter set $\hat{\boldsymbol{\theta}}$ is determined using the event times identified in Section 2.3 (based on $\tilde{\boldsymbol{x}}(t)$), in the optimization of the likelihood function defined in (6). The optimal parameter set is used in defining the intensity function.

We consider two instances of the effect (over time) of the exogenous variables, which lead to different definitions of the intensity function. In the first instance, we consider the effect of the intensity function at some instantaneous time τ_n to obtain (8).

$$I_n \quad = \quad \Lambda(\tau_n|\hat{\boldsymbol{\theta}}) \tag{8}$$

In the second instance, we consider the cumulative effect of the intensity function I_n^*, from τ_{n-1} to τ_n. The integrated intensity function is given by (10).

$$I_n^* \quad = \quad \int_{\tau_{n-1}}^{\tau_n} \Lambda(t|\hat{\theta})dt \tag{9}$$

$$= \quad \hat{\lambda}(\tau_n - \tau_{n-1}) + \frac{\hat{\alpha}}{\hat{\beta}}\left[\sum_{t_i \leq \tau_n}\left(1 - \frac{e^{\hat{\beta}t_i}}{e^{\hat{\beta}\tau_n}}\right) - \sum_{t_i \leq \tau_{n-1}}\left(1 - \frac{e^{\hat{\beta}t_i}}{e^{\hat{\beta}\tau_n}}\right)\right] \tag{10}$$

The series X_n is defined such that $X_n = I_n$ or $X_n = I_n^*$. The specific expression for X_n will be determined for each particular dataset.

3 Summary of Computational Procedures

The computational procedure adopted can be summarized as follows:

1. Optimize $\ell_H(\hat{\boldsymbol{\theta}})$ for MLE estimates, $\hat{\boldsymbol{\theta}}$, of the intensity function, $\Lambda(t|\boldsymbol{\theta})$,
2. Using $\Lambda(t|\hat{\boldsymbol{\theta}})$, generate exogenous variable contributions, X
3. For each model, obtain the LSE $\hat{\boldsymbol{\phi}}$ (eq. (11)) of the AR coefficients, where

$$\hat{\boldsymbol{\phi}} = (X^\top X)^{-1} X^\top Y, \tag{11}$$

$$\boldsymbol{\phi} \equiv \begin{cases} (a_1, \ldots, a_M)^\top, & \text{AR}, \\ (a_1, \ldots, a_M, b_j)^\top, & \text{ARX}, \\ (a_1, \ldots, a_M, b_{1,j}, \ldots, b_{M,j})^\top & \text{mmAR}, \end{cases} \tag{12}$$

$$Y = (B_{M+1}, \cdots, B_N)^\top, \tag{13}$$

and for $j = 1, 2, \ldots$,

$$X = \begin{cases} \begin{pmatrix} B_M & \cdots & B_1 \\ \vdots & \ddots & \vdots \\ B_{N-1} & \cdots & B_{N-M} \end{pmatrix}, & \text{AR}, \\ \begin{pmatrix} B_M & \cdots & B_1 & X_{M+1-j} \\ \vdots & \ddots & \vdots & \vdots \\ B_{N-1} & \cdots & B_{N-M} & X_{N-j} \end{pmatrix}, & \text{ARX}, \\ \begin{pmatrix} B_M & \cdots & B_1 & X_{M+1-j}B_M & \cdots & X_{M+1-j}B_1 \\ \vdots & \ddots & \vdots & \vdots & \ddots & \vdots \\ B_{N-1} & \cdots & B_{N-M} & X_{N-j}B_{N-1} & \cdots & X_{N-j}B_{N-M} \end{pmatrix}, & \text{mmAR}. \end{cases} \tag{14}$$

4. Let $\hat{B}_n$ be the prediction of B_n based on $B_1, \ldots, B_{n-M}$, using the models defined in (7). For each of the models defined in (7), we can derive the prediction error term $\epsilon_n(\phi)$, where ϕ is a vector of the model parameters, and $n = M+1, \ldots, N$. Note that the values and dimension of ϕ will depend on the model choice. The likelihood function $\ell_A(\sigma_\ell^2; \epsilon_{M+1}, \ldots, \epsilon_N, \phi)$ is given by (15), from which we derive the log-likelihood (16).

$$\ell_A(\sigma_\ell^2; \epsilon_{M+1}, \ldots, \epsilon_N, \phi) = \frac{1}{(2\pi\sigma_\ell^2)^\mu} \exp\left\{ - \sum_{n=M+1}^{N} - \frac{\epsilon_n^2(\phi)}{2\sigma_\ell^2} \right\}, \tag{15}$$

$$\log \ell_A(\sigma_\ell^2; \epsilon_{M+1}, \ldots, \epsilon_N, \phi) = -\mu(1 + \log(2\pi\sigma_\ell^2)), \tag{16}$$

$$\mu = (N - M)/2.$$

We base our model selection on the Akaike Information Criterion (AIC), defined by (17)

$$AIC = -2 \times \ell_A + 2 \times (\text{number of parameters}). \tag{17}$$

For each of the three model classes defined in (14), we identify the AIC to determine the optimum time lag M for B, and j for X.

5. Generate mutually independent normal random variables $\epsilon_{N+1}^{(r)}(r = 1,\ldots,R)$ with mean 0 and variance $\hat{\sigma}_\ell^2$, where R is the number of independent iterates in a Monte Carlo simulation, and $\hat{\sigma}_\ell^2$ is the MLE of σ_ℓ^2. Obtain one step ahead prediction for each AR model using $B_n(n = 1,\ldots,N)$ and (18).

$$\tilde{B}_{N+1}^{(r)} = \begin{cases} \sum_{m=1}^{M} \hat{a}_m B_{N-m} + \epsilon_{N+1}^{(r)}, & \text{AR}, \\ \sum_{m=1}^{M} \hat{a}_m B_{N-m} + \hat{b} X_{N-j} + \epsilon_{N+1}^{(r)}, & \text{ARX}, \\ \sum_{m=1}^{M} (\hat{a}_m + \hat{b}_m X_{N-j}) B_{N-m} + \epsilon_{N+1}^{(r)} & \text{mmAR}, \end{cases} \tag{18}$$

where $\hat{a}_m$, $\hat{b}$ and $\hat{b}_m$ are LSE of the parameters.

6. Calculate the prediction confidence intervals $\hat{\mu}_{\text{pre}} \pm 2\hat{\sigma}_{\text{pre}}$, given

$$\hat{\mu}_{\text{pre}} = R^{-1} \sum_{j=1}^{R} \tilde{B}_{N+1}^{(j)}, \tag{19}$$

$$\hat{\sigma}_{\text{pre}} = (R-1)^{-1} \sum_{j=1}^{R} \left(\tilde{B}_{N+1}^{(j)} - \hat{\mu}_{\text{pre}} \right)^2. \tag{20}$$

The κ-steps ahead prediction confidence interval is constructed analogously using $B_1,\ldots,B_N,\tilde{B}_{N+1},\ldots,\tilde{B}_{N+\kappa-1}$.

4 Application — Data and Event Time Detection

We use the net volume flux (inflow minus outflow) of AW, measured along the FB section (see Fig. 1) since 1997, using current-meter morrings.[3, 19]. In this paper, we use the monthly mean value of volume flux data from 1998 to 2014 (see Fig. 2a). Following [3], we consider the fluxes spanning April–July of the considered years as proxies for zooplankton levels in the Barents Sea.

The capelin biomass data (see Fig. 2b) is taken from the database of the Working Group on the Integrated Assessments of the BS (WGIBAR) [17]. Observation data for capelin of age 4+ is usually sparse and unreliable because BS capelin usually spawns at 3 years, and then dies [7]. We shall therefore restrict the analysis and discussion of simulation results to cover capelin in the age range 1–3 years only.

We applied the events identification algorithm described in Section 2.3 to the volume flux data, in order to define the event times $\tau_1,\ldots,\tau_n$. We used a simplified approach in defining the parameters for event detection.

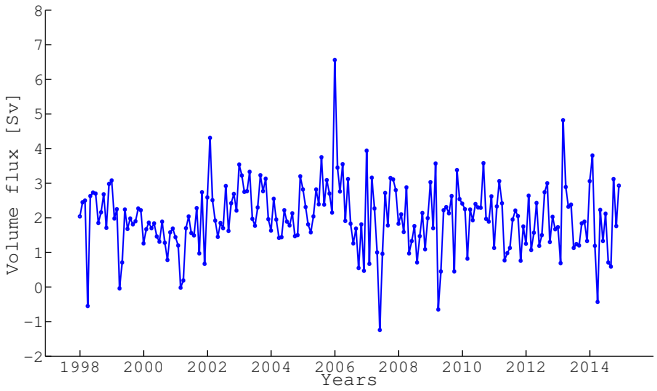

a. Volume flux of AW

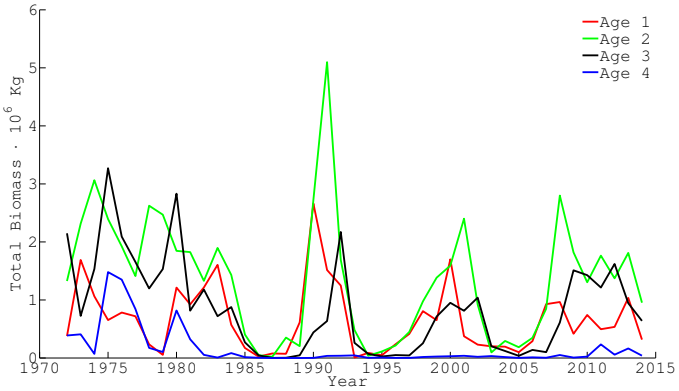

b. Capelin biomass

Figure 2: Monthly mean volume flux of AW (left) and capelin biomass (right).

We set $\psi = 0.25 \cdot \{\max(\boldsymbol{x}) - \min(\boldsymbol{x})\}$, $\omega_1 = 0.080$, and $\omega_2 = 1.001$. where the threshold values for ω were based on the mean and standard deviation for the particular months considered.

Figure 3 shows a plot of the biomasses and event times (triangles).

4.1 Application of Hawkes Process Model to Events Data

We use the flux data to identify the optimal event months. The Maximum Likehood Estimates (MLEs) were obtained using an interior-point optimization algorithm (implemented as fmincon in ©Matlab). The results are summarized in Table 1, where $\hat{\boldsymbol{\theta}}$ (with largest log-likelihood), is given by $\hat{\boldsymbol{\theta}} \equiv (\hat{\lambda}, \hat{\alpha}, \hat{\beta}) \equiv (0.69, 0.52, 11.99)$. This manuscript does not consider the

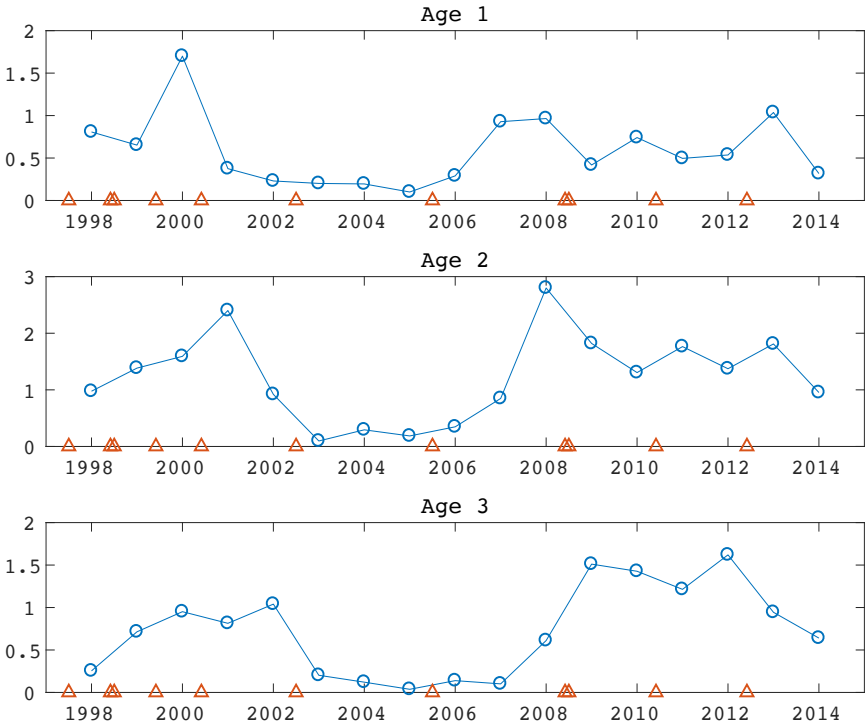

Figure 3: The triangle and blue lines represent estimated event times, and biomass observations, respectively. For each age group, the vertical axis is scaled by $10^{-}6$.

effect of uncertainties in $\hat{\boldsymbol{\theta}}$ on the estimation of other parameters. Figure 4 is the estimated intensity function for March–April, using the largest ML value (see Table 4).

Table 1: The MLE of parameters, and associated maximum log-likelihood values. Data for March–April are optimal for the Hawkes process model.

Month intervals	MLE of parameters			ML
	$\hat{\lambda}$	$\hat{\alpha}$	$\hat{\beta}$	ℓ_H
March–April	0.69	0.52	11.99	-14.55
March–June	1.10	0.00	11.81	-16.25
March–July	1.16	0.00	11.58	-16.13

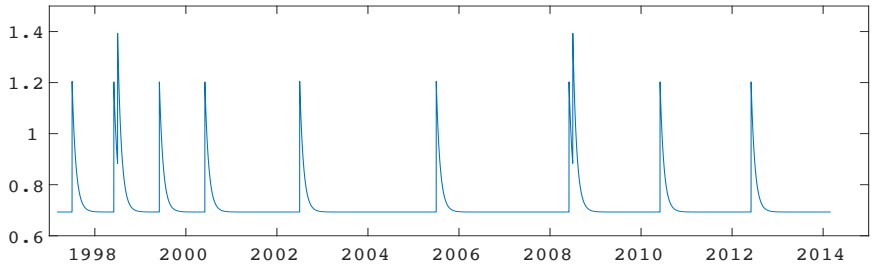

Figure 4: Estimated Intensity function

4.2 Coupling the Intensity Function to Population Dynamics Models

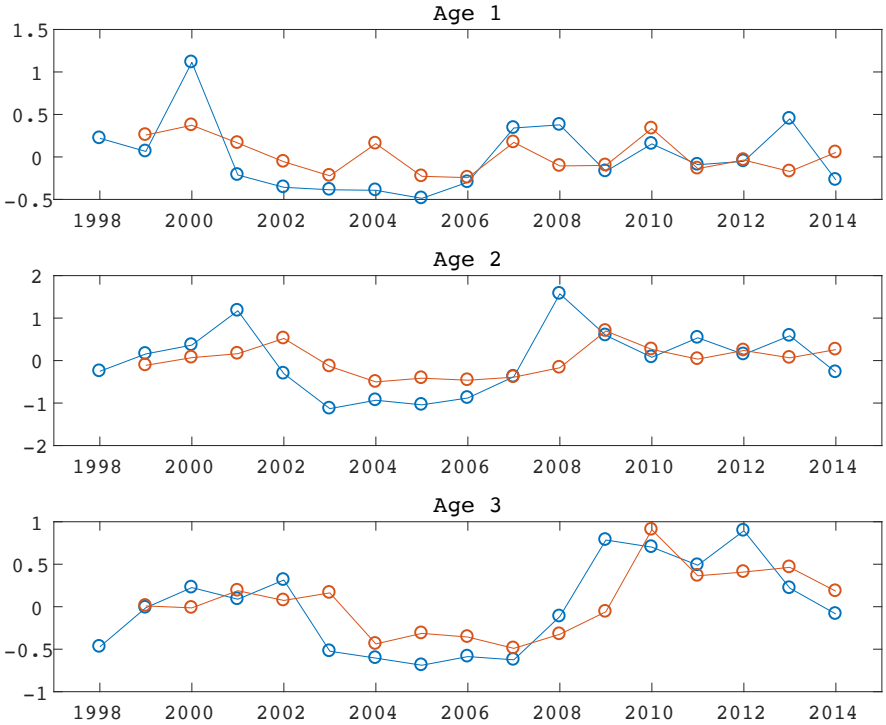

Figure 5: Comparison of best model fit (red) to observation data (blue). The vertical axis is mean-centered and scaled (multiplied by 10^-6) biomass. The scaled mean for ages 1, 2, and 3 are respectively 0.5875, 1.2276 and 0.7259.

Table 2: Summary of model fitting results. The column labels of Age, Var, ML and AIC represent respectively, biomass age, variance of the residual error, log-likelihood, and AIC values. ARX1, and ARX2 are ARX models with respectively, I_n, and I_n^*, and similarly for mmAR1 and mmAR2.

Age	Model	Order	Var	ML	AIC
Age 1	AR	$M = 1$	0.16	-7.79	17.59
	AR	$M = 2$	0.17	-8.75	21.51
	ARX1	$M = 1$	0.12	-3.92	11.84
	ARX1	$M = 2$	0.13	-4.38	14.75
	ARX2	$M = 1$	0.15	-6.56	17.12
	ARX2	$M = 2$	0.14	-6.04	18.09
	mmAR1	$M = 1$	0.16	-7.61	19.24
	mmAR1	$M = 2$	0.15	-7.24	22.48
	mmAR2	$M = 1$	0.15	-6.82	17.63
	mmAR2	$M = 2$	0.14	-6.40	20.80
Age 2	AR	$M = 1$	0.46	-23.70	49.40
	AR	$M = 2$	0.47	-23.87	51.74
	ARX1	$M = 1$	0.46	-23.67	51.35
	ARX1	$M = 2$	0.47	-23.85	53.70
	ARX2	$M = 1$	0.46	-23.47	50.95
	ARX2	$M = 2$	0.47	-23.84	53.68
	mmAR1	$M = 1$	0.46	-23.70	51.40
	mmAR1	$M = 2$	0.47	-23.78	55.56
	mmAR2	$M = 1$	0.46	-23.55	51.10
	mmAR2	$M = 2$	0.46	-23.66	55.33
Age 3	AR	$M = 1$	0.14	-6.32	14.64
	AR	$M = 2$	0.14	-5.72	15.58
	ARX1	$M = 1$	0.14	-6.08	16.15
	ARX1	$M = 2$	0.14	-5.77	17.54
	ARX2	$M = 1$	0.14	-6.30	16.60
	ARX2	$M = 2$	0.13	-5.35	16.69
	mmAR1	$M = 1$	0.13	-5.37	14.73
	mmAR1	$M = 2$	0.13	-4.67	17.34
	mmAR2	$M = 1$	0.12	-4.02	12.04
	mmAR2	$M = 2$	0.12	-3.90	15.80

From Table 2, ARX1 with order $M = 1$ for age 1, AR with order $M = 1$ for age 2, and mmAR1 with order $M = 1$ for age 3, are the best fitting models. Figure 5 shows a comparison of the model fit to data for the indicated ages. We examined the optimal value for j (the degree of lag) in the ARX and mmAR models using the AIC indices. Our results shows that $j = 1$ is optimal for both model instances. Table 2 summarizes the result of applying the AR models to biomass of the respective ages. The models with least AIC value are best fitting models to the data.

4.3 Quantifying Prediction and Prediction Uncertainty

Using the intensity function and best fit models, we performed κ-steps ahead predictions of the biomasses, and quantified the 95% confidence intervals associated with each prediction. With reference to the shaded regions in Figure 6, the lightest gray area (utmost left) represents a $\kappa = 4$ years ahead prediction confidence interval, while the next (light gray) area represents a $\kappa = 1, 2, 3$-steps ahead prediction confidence interval, where data from 1998 to 2011 has been used in the model fitting. The dark gray area (third shaded region counting from left to right) indicates a $\kappa = 1, 2$-steps ahead prediction confidence interval, using fitting data from 1998 to 2012. Finally, the darkest gray area is a $\kappa = 1$-step ahead prediction confidence interval, based on fitted data from 1998 to 2013.

5 Discussion and Summary

This paper has presented a modeling framework within which an environmental driver has been coupled to a population dynamics model, to track the impulsive trajectory of a marine population. To the best of our knowledge, this is the first of such modeling approaches in marine science, that involves using point processes stochastic control techniques in population dynamics modeling.

The use of the volume flux of AW for event detection has been motivated by the fact that inflowing AW plays a crucial role in the physical and ecological conditions of the Barents Sea [18]. The inflowing AW currents ameliorate the winter climate of the polar latitudes [30], and thus influence the growth rate and distribution of zooplankton and fish larvae, as well as fish population parameters as growth, recruitment, migration and distribution (see [14, 24, 32]

Our analysis identified the volume flux of AW during March–April as the optimal events time interval. This result is consistent with earlier studies (see e.g. [3]), which found the early spring (March-April) inflow most important for determining the peak zooplankton density in the FB section during August. The authors in [3] argued that this is linked to the conditions in March-April that determine the initial conditions for plankton transport

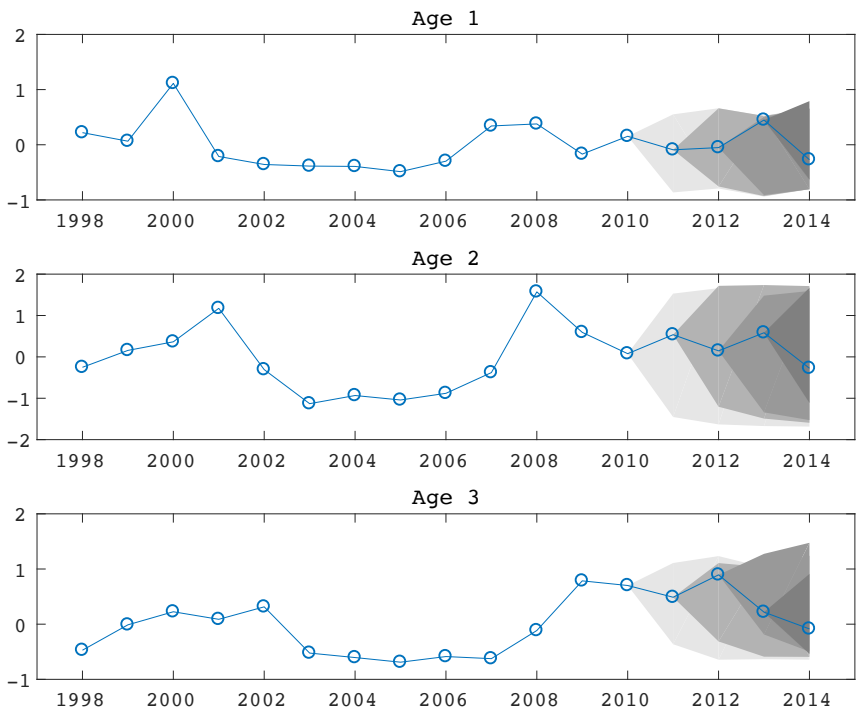

Figure 6: Comparison of observed (blue) and 95% confidence intervals for κ-steps ahead predictions. The nested confidence intervals (from left to right) represent respectively, (i) $\kappa = 4$ (ii) $\kappa = 1, 2, 3$, based on model fit to data from 1998 to 2011, (iii) $\kappa = 1, 2$, based on model fit to data from 1998 to 2012 (iv) $\kappa = 1$, based on model fit to data from 1998 to 2013.

from the Norwegian Sea into the BS, and the development of successive generations that might be produced while being transported northwards in the BS. The modeling process identified three distinct model (see Table 3) types for the various age groups, where X_{n-1} and X^*_{n-1} follow respectively, the definitions in (8) and (9).

Our results show that the dynamics of age-2 capelin biomass is solely determined by a first-order autoregressive process, i.e., by the biomass of the previous year (age-1 fish). To explain this, one must first note that the biomass of age-2 capelin dominates the total stock biomass during the time intervals (see the year intervals 1998–2014, Fig. 2) considered. According to the literature (see [20]), when the stock increases, the higher food demands are met by an expansion of the feeding areas. Furthermore, that the age composition may be a determining factor such that, a stock consisting pre-

Table 3: Summary of identified model types.

Age	Identified model	Parameters
1	$B_n = aB_{n-1} + bX_{n-1} + \epsilon_n$	$a = 0.1663$, $b = 298.3563$
2	$B_n = aB_{n-1} + \epsilon_n$	$a = 0.4437$
3	$B_n = (a + bX^*_{n-1})B_{n-1} + \epsilon_n$	$a = 0.6539$, $b = 259.7213$

dominantly of young capelin may have a more southerly distribution and different migration pattern compared to a stock with a high abundance of older fish [4]. The absence of a direct exogenous forcing on age-2 capelin may therefore be explained by the fact that for this particular age-group, density (secondary) effects (resulting in larger spatial distribution and propensity to longer feeding migration) dominate the dynamics. A spatio-temporal modeling framework that includes an index of spatial distribution as exogenous parameter may be a viable alternative to that examined in this manuscript.

In constrast to age-2 fish, age-1 and age-3 biomasses appear to be affected respectively, by additive and multiplicative forcing. According to the theory (see e.g., [16]), the system response differ depending on whether the forcing is additive or multiplicative. Whereas additive stochastic forcing has a predetermined distribution, multiplicative forcing (such as for age-3 biomass) implies that the stochastic component of the dynamics ($bX^*_{n-1}B_{n-1}$) evolves with the environment, and has the ability to fundamentally change the dynamical characteristics and properties of the population trajectory (see [27]). Observe that in particular for age-3, the biomass dynamics also involves an integrated effect (X^*_{n-1}) of the environment, and its effect on the age-2 biomass (B_{n-1}).

In general, the capelin biomass data for all ages is highly variable because it includes multiple episodes of stock collapse, although our prediction interval (2011–2014) spans a period during which the stock appears to be relatively stable. This relative stability notwithstanding, Fig. 6 shows notable changes in biomass prediction uncertainties (especially for capelin of ages 1 and 3) over different prediction horizons. We also observe that in general, the 95% confidence interval encapsulates the predictions. The highest uncertainty is associated with biomass predictions for age-2 capelin, where the uncertainty envelope remains almost invariant even for short term predictions (even for $\kappa = 1$). The results from Fig. 6 for this age-group are consistent with previous discussions about the limitations of the exogenous observations, as well as the derived model (in Table 3), as tools for predicting age-2 capelin biomass dynamics.

In summary, our results show that the population trajectory of age-1 fish can be tracked by monitoring the exogenous factor (volume flux) considered in this paper. The strong dependence of age-3 biomass dynamics on the

integrated environmental effect on age-2 fish can form the basis for developing a management strategy for sustainable exploitation of this particular species. For instance, if a base-line (*stable* environmental condition) is established, then a metric that quantifies the integrated deviation from the baseline over the last two years may be used to predict the future state (bust-boom) of the stock. This approach (an extension of work presented in this manuscript) will be pursued in further research.

Acknowledgements

This work has been partly funded by the following IMR Research Programs – MarPro-PROVEN (Project # 14412), the Barents Sea Program (Project # 84126) and Reduced Uncertainty in Stock Assessments (REDUS, Project # 14809-01). SS is grateful for research grant from the Fulbright Foundation. The authors are grateful to Anna Frank (University of Oslo, Norway) and Randi Ingvaldsen (Institute for Marine Research, Bergen, Norway) for useful comments. Codes (Matlab and R) for the analysis presented in this paper are available upon request from the corresponding author (SS).

References

[1] B Bogstad and S Mehl. Interactions between cod (gadus morhua) and its prey species in the barents sea. forage fishes in marine ecosystems. In *Proceedings of the International Symposium on the Role of Forage Fishes in Marine Ecosystems*, number 97-01 in Alaska Sea Grant College Program Report, pages 591–615, University of Alaska Fairbanks, 1997.

[2] Pierre Brémaud and Laurent Massoulié. Stability of nonlinear Hawkes processes. *The Annals of Probability*, pages 1563–1588, 1996.

[3] Padmini Dalpadado, Randi B Ingvaldsen, Leif Christian Stige, Bjarte Bogstad, Tor Knutsen, Geir Ottersen, and Bjørnar Ellertsen. Climate effects on Barents Sea ecosystem dynamics. *ICES Journal of Marine Science*, 69(7):1303–1316, 2012.

[4] Per Fauchald, Mette Mauritzen, and Harald Gjøsæter. Density-dependent migratory waves in the marine pelagic ecosystem. *Ecology*, 87(11):2915–2924, 2006.

[5] H Gjøsæter and B Bogstad. Effects of the presence of herring (Clupea harengus) on the stock-recruitment relationship of Barents Sea capelin (Mallotus villosus). *Fisheries Research*, 38(1):57–71, 1998.

[6] H Gjøsæter and N G Ushakov. Capelin in the Barents Sea. In *Proceedings of the 10th Norwegian–Russian Symposium (Bjordal Å, Gjøsæter H and Sigbjørn Mehl, eds.)*, pages 8–17, Bergen, Norway, 2003.

[7] Harald Gjøsæter, Bjarte Bogstad, and Sigurd Tjelmeland. Assessment methodology for Barents Sea capelin, Mallotus villosus (Müller). *ICES Journal of Marine Science*, 59(5):1086–1095, 2002.

[8] Harald Gjøsæter, Bjarte Bogstad, and Sigurd Tjelmeland. Ecosystem effects of the three capelin stock collapses in the Barents Sea. *Marine Biology Research*, 5(1):40–53, 2009.

[9] Harald Gjøsæter, Bjarte Bogstad, Sigurd Tjelmeland, and Samuel Subbey. A retrospective evaluation of the Barents Sea capelin management advice. *Marine Biology Research*, 11(2):135–143, 2015.

[10] Harald Gjøsæter, Elvar H Hallfredsson, Nina Mikkelsen, Bjarte Bogstad, and Torstein Pedersen. Predation on early life stages is decisive for year-class strength in the Barents Sea capelin (Mallotus villosus) stock. *ICES Journal of Marine Science*, page 177, 2015.

[11] Elvar H Hallfredsson and Torstein Pedersen. Effects of predation from juvenile herring (clupea harengus) on mortality rates of capelin (mallotus villosus) larvae. *Canadian Journal of Fisheries and Aquatic Sciences*, 66(10):1693–1706, 2009.

[12] Alan G Hawkes. Spectra of some self-exciting and mutually exciting point processes. *Biometrika*, 58(1):83–90, 1971.

[13] Alan G Hawkes and David Oakes. A cluster process representation of a self-exciting process. *Journal of Applied Probability*, 11(3):493–503, 1974.

[14] K Helle and M Pennington. The relation of the spatial distribution of early juvenile cod (Gadus morhua L.) in the Barents Sea to zooplankton density and water flux during the period 1978-1984. *ICES Journal of Marine Science*, 56(1):15–27, 1999.

[15] D Ø Hjermann, G Ottersen, and N C Stenseth. Competition among fishermen and fish causes the collapse of Barents Sea capelin. *PNAS*, 101(32):11679–11684, 2004.

[16] Werner Horsthemke and René Lefever. *Noise-induced transitions in physics, chemistry, and biology*. Springer, 1984.

[17] ICES. Working Group on the Integrated Assessments of the Barents Sea (WGIBAR). ICES CM 2016/SSGIEA:04, ICES, Murmansk, Russia, 2016.

[18] Randi Ingvaldsen. *The Atlantic inflow to the Barents Sea*. University of Bergen, Department of Geophysical Institute, 2003.

[19] Randi B Ingvaldsen, Lars Asplin, and Harald Loeng. The seasonal cycle in the Atlantic transport to the Barents Sea during the years 1997–2001. *Continental Shelf Research*, 24(9):1015–1032, 2004.

[20] Randi B Ingvaldsen and Harald Gjøsæter. Responses in spatial distribution of Barents Sea capelin to changes in stock size, ocean temperature and ice cover. *Marine Biology Research*, 9(9):867–877, 2013.

[21] Hiroko Kato and Manabu Honda. Multiplicatively modulated exponential autoregressive model for corticomuscular functional coupling. *Signal processing*, 85(7):1287–1300, 2005.

[22] Jesper Møller and Jakob G Rasmussen. Perfect simulation of Hawkes processes. *Advances in applied probability*, 37(3):629–646, 2005.

[23] Thomas M Norman, Nathan D Lord, Johan Paulsson, and Richard Losick. Memory and modularity in cell-fate decision making. *Nature*, 503(7477):481, 2013.

[24] G Ottersen and H Loeng. Covariability in early growth and year-class strength of Barents Sea cod, haddock, and herring: the environmental link. *ICES Journal of Marine Science*, 57(2):339–348, 2000.

[25] Tohru Ozaki. Maximum likelihood estimation of Hawkes' self-exciting point processes. *Annals of the Institute of Statistical Mathematics*, 31(1):145–155, 1979.

[26] Tohru Ozaki. *Time series modeling of neuroscience data.* CRC Press, 2012.

[27] Cristina L Perez, Andrew M Moore, Javier Zavala-Garay, and Richard Kleeman. A comparison of the influence of additive and multiplicative stochastic forcing on a coupled model of ENSO. *Journal of climate*, 18(23):5066–5085, 2005.

[28] Izhak Rubin. Regular point processes and their detection. *IEEE Transactions on Information Theory*, 18(5):547–557, 1972.

[29] Robert H Shumway and David S Stoffer. *Time series analysis and its applications: with R examples.* Springer Science & Business Media, 2006.

[30] Igor Smolyar and N Adrov. The quantitative definition of the Barents Sea Atlantic Water: mapping of the annual climatic cycle and interannual variability. *ICES Journal of Marine Science*, 60(4):836–845, 2003.

[31] Hiroko K Solvang, Sam Subbey, and Anna S Frank. Causal Drivers of Barents Sea Capelin (*Mallotus villosus*) Population Dynamics on Different Time Scales. *ICES Journal of Marine Science*, (In press), 2017.

[32] Nils C Stenseth, Atle Mysterud, Geir Ottersen, James W Hurrell, Kung-Sik Chan, and Mauricio Lima. Ecological effects of climate fluctuations. *Science*, 297(5585):1292–1296, 2002.

[33] Harald Yndestad and Anne Stene. System dynamics of the Barents Sea capelin. *ICES Journal of Marine Science*, 59(6):1155–1166, 2002.

[34] Harald Yndestad, William R Turrell, and Vladimir Ozhigin. Lunar nodal tide effects on variability of sea level, temperature, and salinity in the Faroe-Shetland Channel and the Barents Sea. *Deep Sea Research Part I: Oceanographic Research Papers*, 55(10):1201–1217, 2008.

Received October 2017; revised August 2018.